Atmospheric Environment 43 (2009) 734–748

Contents lists available at ScienceDirect

Atmospheric Environment

journal homepage: www.elsevier.com/locate/atmosenv

Influence of wall roughness on the dispersion of a passive scalar in a turbulent boundary layer

P. Salizzoni [a,b,*], R. Van Liefferinge [a], L. Soulhac [a], P. Mejean [a], R.J. Perkins [a]

[a] Laboratoire de Mécanique des Fluides et d'Acoustique, Université de Lyon CNRS, École centrale de Lyon, INSA Lyon, Université Claude Bernard Lyon I, 36, avenue Guy de Collongue, 69134 Ecully, France
[b] Dipartimento di Ingegneria Aerospaziale, Politecnico di Torino, Corso Duca degli Abruzzi 24, Torino, Italy

ARTICLE INFO

Article history:
Received 21 December 2007
Received in revised form 23 July 2008
Accepted 24 July 2008

Keywords:
Passive scalar dispersion
Roughness
Urban canopy
Turbulent boundary layer

ABSTRACT

Many towns and cities consist of similarly sized buildings in relatively regular arrangements with smaller scale roughness elements such as roofs, chimneys and balconies. The objective of this study is to investigate how small scale roughness elements modify the influence of the large scale organized roughness on the dispersion of a passive scalar in a turbulent boundary layer. Wind tunnel experiments were performed using a passive tracer released from a line source and concentration profiles were measured with a Flame Ionisation Detector. The measurements are compared with numerical solutions of the advection–diffusion equation.

The results show that decreasing the cavity aspect ratio increases the turbulent vertical mass fluxes, and that the small scale roughness enhances these fluxes, but only in the skimming flow regime. Numerical simulations showed that outside the roughness sublayer (RSL) the changes in surface roughness could be accounted for by a simple variation of the friction velocity, but inside the RSL the spatial variability of the flow imposed by the roughness elements has much more influence. A simple model for a spatially averaged dispersion coefficient in the RSL has been developed and is shown to agree satisfactorily with the concentrations measured in these experiments.

1. Introduction

Pollutant emissions within the urban canopy have a significant influence on urban air quality, and it is therefore important to understand how pollutants are transported and mixed within the urban canopy. This depends strongly on the turbulence in the lower part of the boundary layer, which in turn is influenced by the interaction between the wind and the obstacles which determine the effective roughness of the urban surface. It is often assumed that an urban area acts on the overlying boundary layer simply as a very rough surface, and there have been many studies of the general problem of the dispersion of a passive scalar in a rough wall boundary layer (Fackrell and Robins, 1982; Raupach and Coppin, 1983; Coppin et al., 1986). Various theoretical models have been developed for dispersion from ground level sources in rough wall boundary layers, but these all require empirical corrections to give satisfactory results (Britter and Hanna, 2003).

In many urban areas the buildings tend to be of similar size, to be spaced rather regularly, and with a characteristic height H that can be a significant fraction of the boundary layer depth δ. So scalings obtained from similarity theory, which assumes $\delta > h_s$, where h_s is some 'effective roughness length' (Nikuradse, 1933), do not necessarily apply to urban areas (Jiménez, 2004). The geometrical organization of

* Corresponding author. Laboratoire de Mécanique des Fluides et d'Acoustique, Université de Lyon CNRS, École centrale de Lyon, INSA Lyon, Université Claude Bernard Lyon I, 36, avenue Guy de Collongue, 69134 Ecully, France. Tel.: +33 4 72186507.
E-mail address: pietro.salizzoni@polito.it (P. Salizzoni).

1352-2310/$ – see front matter © 2008 Elsevier Ltd. All rights reserved.
doi:10.1016/j.atmosenv.2008.07.057

large obstacles in the urban boundary layer can also influence turbulent fluxes in a way in which random surface roughness does not (e.g. Davidson et al., 1995). There have therefore been a number of studies aimed at characterizing the dynamics of the roughness sub-layer (RSL) in urban areas and forest canopies (Thom, 1971; Garratt, 1978; Raupach et al., 1986; Rotach, 1995; Kastner-Klein et al., 2004). Some studies have also been devoted specifically to the question of the dispersion of pollutants in these flows, and these were recently reviewed by Britter and Hanna (2003).

The aim of this study is to investigate the influence of wall roughness on the dispersion of a passive pollutant in a neutral boundary layer. It is well known that in these flows the aspect ratio H/W (W is the spacing between the buildings) has a significant influence on the flow regime, and it can be expected that it ought therefore to affect the dispersion of a pollutant. In real life the roughness of the large-scale elements is modified by the presence of smaller scale elements such as roofs, chimneys and balconies, so we investigate here how the addition of small scale roughness modifies the influence of the large-scale obstacles. Detailed measurements of the velocity field have already been published in Salizzoni et al. (2008); here we investigate the influence of wall roughness on the dispersion of a passive tracer. Concentration profiles have been measured for different source positions and roughness configurations, and the results have been analysed using a combination of analytical and numerical models.

The experimental arrangements and measurement techniques are described in Section 2; the mathematical model and associated numerical methods are presented in Section 3, and the main properties of the velocity field, which were presented in detail in Salizzoni et al. (2008) are summarised in Section 4. Experimental and numerical results are presented and discussed in Section 5.

2. Experimental set up

The experiments were performed in a closed-circuit wind tunnel at the Laboratoire de Mécanique des Fluides et d'Acoustique at the École centrale de Lyon. The test section of this tunnel measures 9 m in length, 1 m in height and 0.7 m in width.

The boundary layer was generated using the method suggested by Irwin (1981), with four spires, 0.4 m high, upstream of the test section. Square section bars (60 mm × 60 mm) were placed normal to the wind, as shown in Fig. 1, to simulate an idealised set of street canyons. The aspect ratio of the cavities between the bars could be varied, and measurements have been performed for three configurations ($H/W = 1$, 2 and 1/2 – Configurations 1, 2, and 3, respectively). The first two configurations correspond to skimming flow and the third to wake-interference flow (Oke, 1988). The influence of roughness at roof level was investigated by adding small 2D roughness elements (5 mm × 5 mm) to the tops of the bars. In all three configurations the experiments were carried out first without small scale roughness – Configurations 1a, 2a and 3a – and then with it – Configurations 1b, 2b, 3b. The properties of the boundary layer in the test section are described in detail in Salizzoni et al. (2008) and summarised briefly in Section 4 of this paper.

Experiments were carried out with a line source located at heights $z_s = 2H$ and $z_s = 3H$ above the ground, as shown in Fig. 2a. The elevated line source (Fig. 2b) was based on devices used by Kitabayashi et al. (1976) and Builtjes (1984). It consists of a supply manifold (external diameter 5 mm) feeding 3 cm long hypodermic needles (internal diameter of 0.25 mm) fitted at intervals of 10 mm. The device was fixed in the wind tunnel with the needles pointing downstream. The tracer gas supply was monitored continuously, using a Brooks flow meter, and the experiments were performed with a mass flux $\dot{M} = 8.43$ mg s^{-1}, giving a mass flow rate per unit length $\dot{M}_q$ equal to 12 mg s^{-1} m^{-1}. The fluctuations in the mass flow rate were less than 1%. The source was first tested in a uniform velocity field to verify that the emission was homogeneous in the spanwise direction, and that the emitted plume was truly two-dimensional.

Even at the lowest source position ($z_s = 2H$) the wake from the source did not modify the turbulence at the level of the tops of the obstacles. Calculations of the growth of the wake behind the cylinder suggest that the width of the wake becomes comparable with the width of the diffusion plume from a point source at a dimensionless distance [$x/(\delta - H)$] downstream of the source which varies for each configuration, but which is always less than 1.6. This means that all the profiles presented here have been measured in the region in which the plume spread is dominated by turbulent diffusion in the boundary layer, rather than by the growth of the wake behind the cylinder.

Fluid velocities were measured by hot-wire anemometry, with a single wire probe and an X-wire probe. Scalar

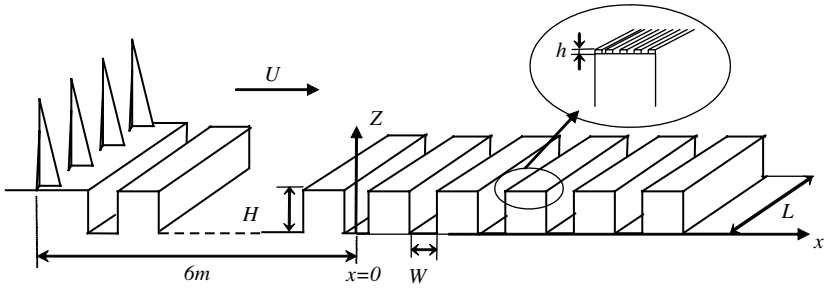

Fig. 1. Overview of the wind tunnel installation. The base of the spires is at $z = H$.

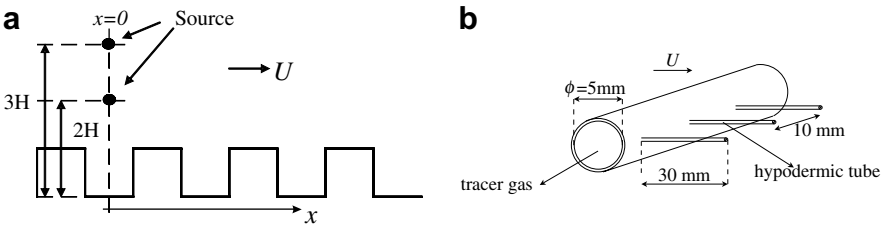

Fig. 2. a) Source position; b) Source characteristics.

concentrations were measured using a Flame Ionisation Detector (FID), with ethane (C_2H_6) as the passive tracer. The FID sampling tube was approximately 25 cm long, which limited the frequency response of the instrument to about 300 Hz (Fackrell, 1980). The errors in the measured values of the mean concentrations are estimated to be less than 1%, based on the measured values of concentration fluctuations, and the number of values used to computed the mean concentration.

Calibration drift of the FID was checked by computing the quantity

$$\dot{M}_1 = \int_0^{\delta} \overline{u}(z)\overline{c}(z)dz$$

from the measured profiles of average velocity $\overline{u}(z)$ and concentration $\overline{c}(z)$. This term is approximately equal to the total average mass flux per unit width across a vertical section of the wind tunnel, given by:

$$\dot{M}_q = \int_0^{\delta} [\overline{u}(z)\overline{c}(z) + \overline{u'c'}]dz$$

where $\overline{u'c'}$ is the turbulent mass transfer in the streamwise direction. The total mass flux $\dot{M}_q$ must be conserved; the approximation to the total mass flux given by $\dot{M}_1$ will also be conserved, provided that $\overline{u'c'} \ll \overline{u}(z)\overline{c}(z)$, that the flow and dispersion are essentially two-dimensional along the streamwise axis and that there is no drift in the hot-wire used to measure the fluid velocities. It was not possible to measure $\overline{u'c'}$ directly, but this term is typically several orders of magnitude smaller than $\overline{u}(z)\,\overline{c}(z)$ (Coppin et al., 1986). Spanwise profiles of mean horizontal velocity (Fig. 4a) and concentration show that they are independent of spanwise distance over most of the cross-section, and the velocity profiles at the upstream and downstream ends of the test section were measured at the beginning and end of each set of experiments to check that there had not been any drift in the anemometer. It therefore seems reasonable to conclude that $\dot{M}_1$ should be conserved with streamwise distance and with time, that any variation in $\dot{M}_1$ will be due to drift in the FID calibration, and that the invariance of $\dot{M}_1$ can be used to correct the drift.

Vertical profiles of fluid velocity and tracer concentration were measured at various distances downstream of the source; velocity profiles were measured both on the centreline of the cavity and over the top of the obstacles whilst each concentration profile was located on the centreline of a cavity. Some examples of the concentration profiles are shown in Fig. 3 for the obstacle Configuration 3a. The most upstream measurement point was located about 6 m downstream of the vortex generators; this is more than 12 times the height of the spires, and is sufficient to ensure that the turbulent structures generated by the spires have reached a quasi-equilibrium state. As a result the change in the boundary layer depth $\Delta\delta$ over the test section is small compared with the boundary layer thickness δ.

3. Mathematical model and numerical methods

We consider a line source of a passive scalar, discharging into a steady turbulent flow, with mean velocity profile $\overline{u}(z)$. We assume that the flow properties do not vary with the downstream distance, that there is no variation in the spanwise direction, that the effects of the molecular diffusion are negligible and that the turbulent fluxes can be

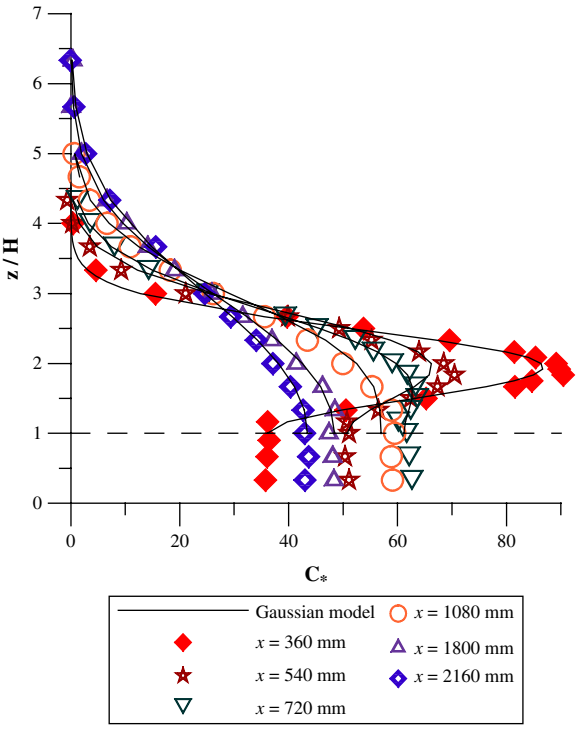

Fig. 3. Vertical profiles of mean concentration at increasing distances downwind of the source ($z_s = 2H$) for Configuration 3a. The continuous lines illustrate the concentration profiles obtained by fitting Eq. (5) to the data, as described in Section 5. The dashed line indicates the top of the obstacles.

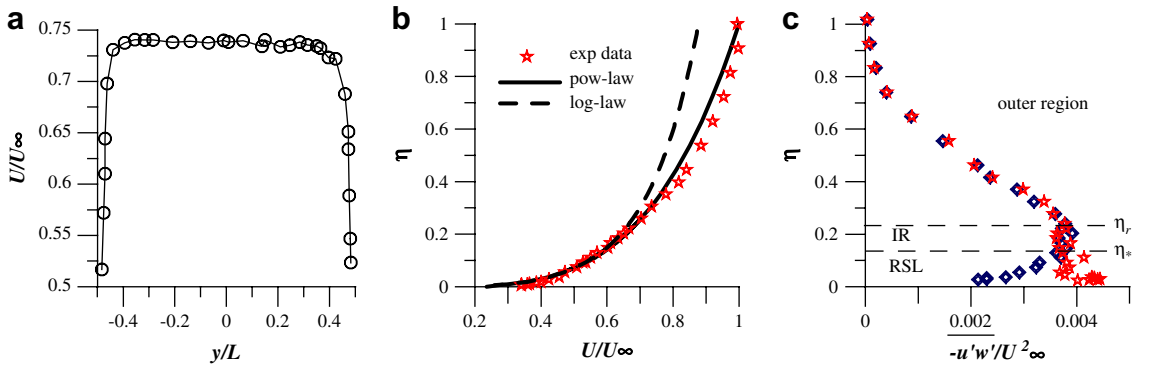

Fig. 4. Velocity field for Configuration 3a. a) Spanwise profile of the mean horizontal velocity at $z = 3H$. b) Vertical profile of the mean horizontal velocity. c) Vertical profiles of Reynolds stress, measured at the cavity centre (stars) and above an obstacle (diamonds).

modelled by a gradient diffusion term with a diffusivity $K(z)$ which depends only on the vertical position z. Strictly speaking K should also depend on x, to model the near-field correctly, but we will be comparing the results with experimental profiles measured far enough downstream that K has become independent on x, so we would have no way of inferring or testing the dependence on x from our measurement. The time-averaged advection–diffusion equation can therefore be written as:

$$\overline{u}\frac{\partial \overline{c}}{\partial x} + \frac{\partial}{\partial z}K\frac{\partial \overline{c}}{\partial z} = 0 \qquad (1)$$

We have assumed that this equation can be applied to the experiments presented here, and we have solved it numerically, using a velocity profile $\overline{u}(z)$ obtained by fitting an analytical curve to the measured velocities, as described in Section 4.

To solve Eq. (1) numerically, we first write the equation in dimensionless form, using normalised vertical (η) and horizontal (ξ) co-ordinates, where:

$$\eta = \left(\frac{z-H}{\delta-H}\right) \quad \xi = \left(\frac{x}{\delta-H}\right)$$

The normalised version of Eq. (1) then becomes:

$$U^{+}\frac{\partial}{\partial \xi}\overline{c} + \frac{\partial}{\partial \eta}K^{+}\frac{\partial \overline{c}}{\partial \eta} = 0 \qquad (2)$$

where $U^{+}(\eta) = \overline{u}(z)/U_{\infty}$ and $K^{+}(\eta) = K(\eta)/[U_{\infty}(\delta - H)]$.

With this normalisation the lower limit of the computational domain $\eta = 0$ is fixed at the obstacle top, i.e. at $z = H$. The definition of the position of the lower boundary is not simple – many previous studies (e.g. Belcher et al., 2003) have shown that the origin of the velocity profiles should be taken at the displacement height d rather than at the top of the obstacles, so it could be argued that the displacement height should also define the lower boundary of the concentration field. But there are also good physical arguments for applying the boundary condition of zero vertical flux ($\partial\overline{c}/\partial\eta = 0$) at the top of the obstacles, rather than at the displacement height. Over the obstacles themselves, the boundary condition must apply at the top of the obstacles (i.e. at $z = H$). Over the cavities between the obstacles it would be possible, in principle, to have a net flux into or out of the cavity. But in steady state conditions the concentration within the cavities must be constant with time, and since the flow is assumed to be two-dimensional, and the cavities are not connected to each other in any way, there can be no net diffusive flux of pollutant into or out of the cavity. Measurements of the velocity field above a cavity show that the mean streamlines do not penetrate into the cavity, so there is no mean advective transport of pollutant across the surface $z = H$ (Salizzoni, 2006). The vertical profiles of concentration plotted in Fig. 3 show that this is true even for wake-interference flow; at all distances downstream of the source, the concentration within the cavity is uniform with height, and the concentration gradient at the top of the cavity ($z = H$) is equal to zero.

Eq. (2) was solved using a pseudo-temporal finite volume method, iterating until the solution converged to a stationary state. The advection term was integrated with an explicit forward-in-time scheme (Bott, 1989a,b; Thuburn, 1997), and the diffusion term was computed by the semi-implicit Crank–Nicholson scheme (solved by the Thomas algorithm). The boundary conditions were defined as follows:

- at the outlet, a Neumann condition was imposed:

$$\frac{\partial \overline{c}}{\partial \xi} = 0$$

- at the lower ($\eta = 0$) and upper ($\eta = 1$) boundaries of the domain, a Neumann condition was also used:

$$\frac{\partial \overline{c}}{\partial \eta} = 0$$

- at the inlet boundary, a Dirichlet boundary condition was set

$$\overline{c} = \overline{c}(\eta)$$

where the function $\overline{c} = \overline{c}(\eta)$ was obtained by fitting a double Gaussian profile (Eq. (5)) to the measured profile.

The results presented here were obtained using a grid of 10 626 cells; to verify that the results were independent of the grid resolution we also repeated some simulations with a grid of 1067 220 cells, and the results were identical. We therefore conclude that the coarser resolution is adequate for these simulations.

4. Flow field

The configurations used in these experiments are similar to those reported in Salizzoni et al. (2008), which provides a detailed description of the wind field. The only major difference between those experiments and the ones reported here concerns the number and dimension of the spires at the entrance to the test section. The experiments in Salizzoni et al. (2008) were performed with 3 spires, each 500 mm high, whereas here we have used 4 spires, each 400 mm high. By reducing the dimensions of the spires we managed to generate a turbulent boundary layer in quasi-equilibrium (i.e. $\delta \simeq$ const) over a large part of the test section. This was verified by comparing velocity profiles measured at $x = 0$ and at $x = 2600$ mm (close to the end of the test section). In these conditions the depth of the boundary layer was equal to about 500 mm (compared with 600 mm for 3 spires), and it remained constant over a distance equal to about five times the depth. So in the region above the roughness sub-layer the distance downstream of the source is the only relevant streamwise scale for the dispersion of a passive scalar.

For all other aspects the two velocity fields are similar and all the features discussed in Salizzoni et al. (2008) apply here. The mean flow is two-dimensional (Fig. 4a) and the vertical profiles of the mean horizontal velocity are independent of the streamwise coordinate, i.e. $U = U(z)$. In the lower part of the domain, the vertical profile of the mean velocity has a logarithmic form (Fig. 4b):

$$\frac{\overline{u}(z)}{u_*} = \frac{1}{\kappa} \ln \frac{(z-d)}{z_0} \tag{3}$$

For each profile, the value of the friction velocity $u_* = \sqrt{-\overline{u'w'}}$ was estimated from the average value of $\overline{u'w'}$ in the inertial region (IR) (Fig. 4c), and the roughness length z_0 and the displacement height d were obtained by fitting the logarithmic profile to the measured vertical velocity profile, by the method of least squares, using the previously-estimated value of u_*. The values of these parameters, for each configuration, are given in Table 1; the uncertainties in the estimations of these parameters are discussed in detail in Salizzoni et al. (2008).

We divide the flow field into three-layers – the roughness sub-layer (RSL), the inertial region (IR) and the outer region – as shown in Fig. 4c. The inertial region is defined as the layer over which the Reynolds stresses are constant; the upper limit of this layer is referred to as z_r and the lower limit is referred to as *blending height* z^*, defined as the lower limit of the constant stress region. The normalised forms of these heights $\eta_r = (z_r - H)/(\delta - H)$ and $\eta^* = (z^* - H)/(\delta - H)$, are given in Table 1. These values show that the addition of small scale roughness does not change the thickness of either the RSL or the IR, but the thickness of these layers depends on the large scale roughness; as it increases, η^* and η_r both tend to increase, but at different rates, so that the thickness of the IR $= \eta_r - \eta^*$ actually decreases.

Table 1
Wind field parameters – $U_\infty = 6.75$ ms^{-1}, $\delta = 500$ mm , $H = 60$ mm

	Configuration (H/W)	z_0/δ	u_*/U_∞	d/H	δ/h_s	n	$\eta_* = \frac{z_*-H}{\delta-H}$	$\eta_r = \frac{z_r-H}{\delta-H}$
1a	(1)	0.00062	0.049	0.95	53.22	0.18	0.022	0.136
2a	(2)	0.00026	0.044	0.98	126.92	0.17	0	0.136
3a	(1/2)	0.0034	0.061	0.87	9.70	0.26	0.136	0.22
1b	(1)	0.0018	0.053	1.02	27.96	0.23	0.022	0.136
2b	(2)	0.0007	0.050	1.02	47.14	0.21	0	0.136
3b	(1/2)	0.0034	0.06	0.87	9.70	0.26	0.136	0.22

The values of the effective roughness length h_s have been calculated from the roughness length assuming that $h_s = 30 z_0$ (Jiménez, 2004). Although the ratio δ/h_s is far from the asymptotic conditions required by similarity theory, the scaling of the velocity profiles agrees well with that given by similarity theory (Salizzoni et al., 2008) – the turbulence above the obstacles depends only on u_*, δ and $(z-d)$. This is true for almost the entire depth of the boundary layer, except for the lowest part in the RSL.

The velocity profile can also be modelled using a power law of the form:

$$\frac{\overline{u}(z)}{U_\infty} = \left(\frac{z-H}{\delta-H}\right)^n \tag{4}$$

which has the advantage over the logarithmic profile of providing a better approximation to the velocity profile in the outer part of the boundary layer, as illustrated in Fig. 4b. We have therefore used this form for the velocity profile in our numerical simulations, with the values of n obtained from a least squares fit to the measured velocities; the computed values of n are given in Table 1. Strictly speaking, it would be more appropriate to use the displacement height d (rather than H) for the origin of the velocity profiles, and since the velocity profile is imposed in our numerical model there is no practical impediment to the use of d. But a comparison of the velocity profiles obtained by fitting the power-law profile to the data showed that there was so little difference in the profiles obtained with the two origins that we have chosen, for convenience, to assume a common origin at $z = H$.

5. Experimental and numerical results

Vertical profiles of mean concentration have been measured at different distances downwind of the source. The results for Configuration 3b are very similar to those of Configuration 3a and so are not plotted here. In all the figures the concentrations are expressed in normalised form:

$$C_* = \overline{c}\, U_\infty (\delta - H)/\dot{M}_q$$

As can be seen in Fig. 5a, the mean concentration at the source height z_s does not vary significantly with the wall

roughness; the spread in centreline concentrations close to the source does not correlate with roughness values, or with possible differences in the mean velocity at source height. However, the concentrations at the height of the obstacles vary significantly with the roughness configuration, as can be seen in Fig. 5b, for a source located at $z_s = 2H$.

To quantify the vertical spread of the plume as a function of distance downstream from the source we have assumed that the vertical concentration profile at any streamwise position can be modelled using a Gaussian profile with an image source to account for the presence of a solid boundary:

$$\overline{c}(x,z) = \frac{\dot{M}_q}{\sqrt{2\pi}\sigma_z U}\left[\exp\left\{-\frac{(z-z_s)^2}{2\sigma_z^2}\right\} + \exp\left\{-\frac{(z+z_s)^2}{2\sigma_z^2}\right\}\right] \quad (5)$$

where $\dot{M}_q$ is the mass flow rate per unit length, z_s is the source height and σ_z is the vertical spread. This profile is a solution of the simplified advection–diffusion equation (Eq. (1)) for the idealised case of a pollutant dispersing in a uniform mean flow with homogeneous turbulence. Although the conditions in these experiments are significantly different, Eq. (5) provides a robust method for estimating values of σ_z, and hence quantifying the effects of surface roughness. To obtain an estimate of σ_z, the theoretical concentration profile Eq. (5) has been fitted to the measured profiles using the method of least squares, and taking the velocity at the source height $(U = \overline{u}(z_s))$. The regression coefficients R^2 obtained using this approach are greater than 0.87 in all cases.

The profiles of plume spread for the different configurations (Fig. 6a) show that the spread increases as the cavity aspect ratio H/W decreases; this corresponds to an increase in the spacing between the obstacles (since H is kept constant) and therefore to an increase in the effective roughness length h_s, as can be seen from Table 1. Physically, an increase in the obstacle spacing enhances turbulent mixing in the boundary layer, and thus increases the turbulent diffusivity, leading to larger values of σ_z. The same argument also explains the effect of adding small scale roughness, which increases turbulent mixing, and results in larger values of σ_z. There is an important limit to this effect, though. Velocity measurements (Salizzoni et al., 2008) show that the addition of small scale roughness increases turbulent intensities for cavity aspect ratios greater than 1 (Configuration 1 and Configuration 2) but once the aspect ratio falls below 1 (Configuration 3), the cavities become so wide that the influence of the small scale roughness is greatly reduced. This is reflected in the fact that the roughness lengths for Configurations 3a and 3b are the same (Table 1) and that the plume spread for Configurations 3a and 3b is identical.

The influence of the diffusivity on the plume spread can also be seen in the way in which σ_z varies with source height (Fig. 6b); as the source height decreases the vertical spread increases, and this is equally true for configurations with and without the small scale roughness (1b and 1a respectively). However it should be remembered that as the source height decreases, the plume is dispersing in a flow with an increasingly strong mean shear; the velocity gradient itself will contribute to spreading the plume, and will increase the effectiveness of the small scale turbulence in the flow (Taylor, 1954).

5.1. Numerical simulations

In order to investigate the effects of inhomogeneity in the mean flow and the turbulence on the dispersion of a plume of a passive scalar we have simulated the experiments, solving Eq. (2) numerically and using the measured profile for the mean velocities. It is also necessary to supply

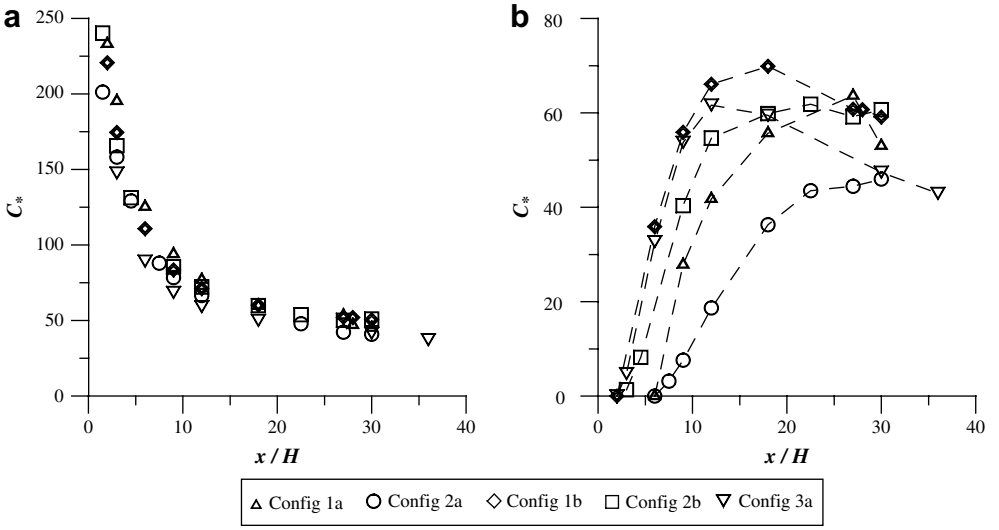

Fig. 5. Streamwise evolution of the mean concentration for an elevated line source ($z_s = 2H$); a) mean concentration at the source height $z = z_s$; b) mean concentration at the obstacle top $z = H$.

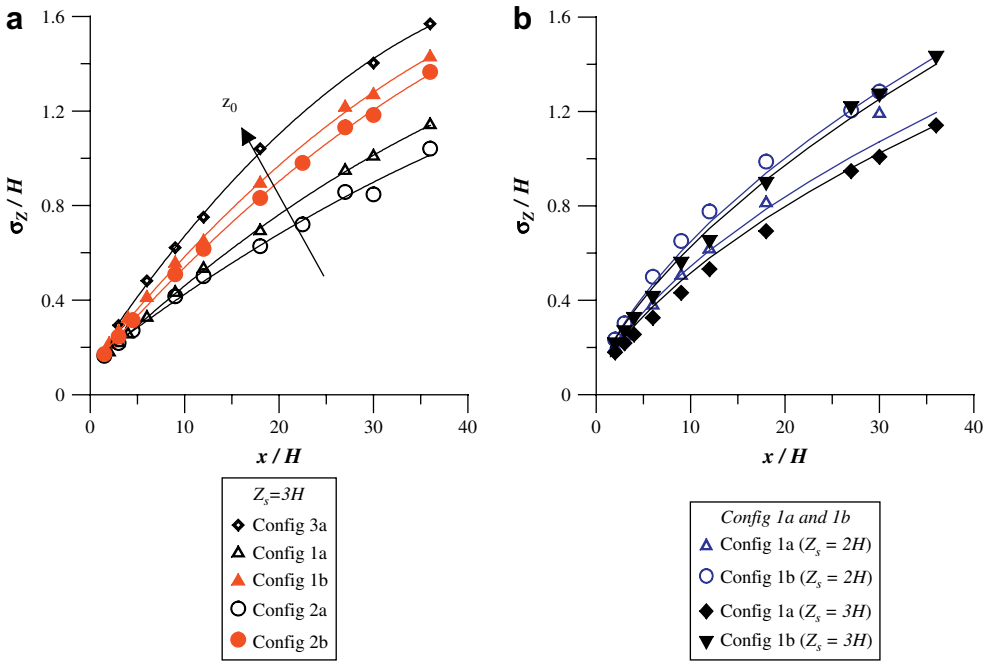

Fig. 6. a) Plume spreading for increasing distances from the source for $z_s = 3H$. b) Effect of the source height on the plume spread: Configurations 1a and 1b. The experimental points are fitted by means of a 2nd order polynomial.

a profile for the dispersion coefficient; in general, this can be expressed as the product of a velocity and a length scale:

$$K(z) = \upsilon(z)\ell(z)$$

so the problem consists of finding the most suitable velocity and length scales for diffusion in a rough boundary layer, and investigating how those scales depend on surface roughness.

Physical reasoning (Belcher et al., 2003) suggests that, close to the wall, $K(z)$ should scale on the friction velocity u_* and on a length scale ℓ, which will be related either to the distance from the top of the obstacles (z–H) or to the size of the roughness elements H. Further away from the wall, $K(z)$ should approach a constant value, scaling on the friction velocity and the boundary layer depth (δ–H). There are some measurements in the atmospheric boundary layer (Clarke, 1970) as well as in wind tunnels that support this scaling (Fackrell and Robins, 1982). Based on these arguments we have divided the boundary layer into two regions – a lower region which extends from the top of the obstacles to the upper limit of the inertial region ($0 < \eta < 0.15$) and an outer region ($0.15 < \eta < 1$), so $K^+(\eta)$ then takes the form (Fig. 13):

$$0 < \eta < \eta_1 \quad K^+(\eta) = \kappa \frac{u_*}{U_\infty} \eta \tag{6}$$

$$\eta_1 < \eta < 1 \quad K^+ = \alpha \frac{u_*}{U_\infty} \tag{7}$$

where κ is the von Kármán constant, α is another constant, to be determined, and $\eta_1 = \alpha/\kappa$ is determined from continuity of the diffusion coefficient. According to wall similarity theory, α should be constant for all boundary layer flows, provided that the ratio δ/h_s is sufficiently large (Jiménez, 2004). This is equivalent to saying that conditions in the outer region are independent of the details of the surface roughness, provided that the boundary layer depth is very much thicker than the effective roughness length. In our experiments the ratio δ/h_s (see Table 1) is large (particularly in Configurations 1 and 2) but not really large enough to ensure that wall similarity applies. So we can expect that α will take similar values for Configurations 1 and 2, but that it might take a different value for Configuration 3. The value of α was determined by performing simulations with a range of different values, and selecting the one that gave best agreement with the measured profiles. On this basis we obtained – for Configurations 1 and 2 – $\alpha = 0.05 \pm 0.005$ which agrees well with the values proposed by Clarke (1970). The corresponding value of η_1 is 0.125 which is close to the value for the outer limit of the inertial layer ($\eta_r = 0.136$) obtained from measurements of the Reynolds stress (Table 1).

In this model we also assume that the diffusion coefficient remains constant throughout the external region of the boundary layer, rather than decreasing as the turbulent intensity diminishes to the free stream value. But we have verified that the results of the simulations are not sensitive to the value of the dispersion coefficient in the upper part of the outer region ($\eta > 0.8$) and this is because most of the plume spreading is confined to the lower part of the boundary layer ($\eta < 0.8$).

It is worth noting that this decomposition of the domain neglects the presence of the RSL in the lower part of the boundary layer, i.e. between the top of the obstacles and the blending height. This implies that the dispersion coefficient is a function of the vertical coordinate η only.

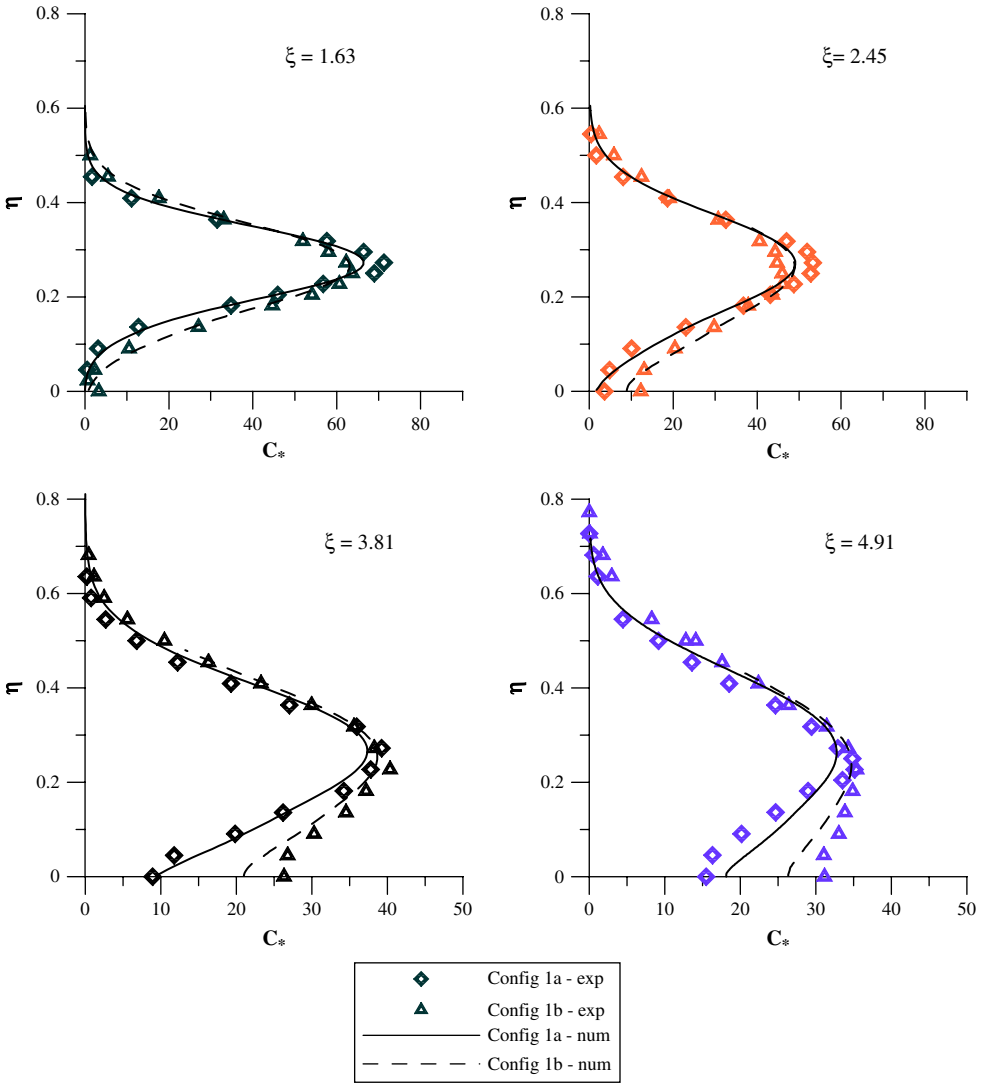

Fig. 7. Vertical profiles of concentration. Configurations 1a and 1b; source position $z_s = 3H$.

The computed concentration profiles are plotted in Figs. 7–12 together with the data.

The vertical profiles of concentration for Configuration 1 are plotted in Fig. 7 ($z_s = 3H$) and Fig. 8 ($z_s = 2H$) together with the results of the numerical simulations. In all cases the addition of small-scale roughness enhances the diffusion close to the top of the obstacles, and increases ground level concentrations. For a source height ($z_s = 2H$) this effect is most noticeable close to the source ($\xi = 1.63$ and $\xi = 2.45$) because the concentration gradient at ground level is greatest at these positions. As the distance from the source increases, the concentration profile close to the top of the obstacles becomes almost uniform, and the thickness of this layer increases with distance. The growth of this layer is related to the rate at which pollutant is mixed down to the ground, and hence to the diffusivity close to the top of the obstacles. Close to the source this layer is much thicker for Configuration 1b, indicating that the small-scale roughness has increased the diffusion significantly. Further downstream the two profiles become similar, because the diffusivity for the case without small-scale roughness has had time to act on the pollutant. The two profiles of measured concentration are closest for $\xi = 3.81$. The addition of small-scale roughness also results in an increased diffusion above the plume centreline, most notably close to the source ($\xi = 1.63$ and $\xi = 2.45$). This effect is in fact due to the way in which the small scale roughness modifies the mean velocity profile, so it is really due to the influence of small scale roughness relatively far upstream of the source; the addition of the small scale roughness reduces the velocities close to the top of the obstacles (the exponent n in the velocity profile increases from 0.18 to 0.23) so that the travel time of the pollutant from the source to the measurement position increases. The diffusion scales on the friction velocity, which increases with increasing roughness, so that the two effects combine to increases the plume spread above the plume centreline as well as close to the top of the obstacles. The increased diffusion away from

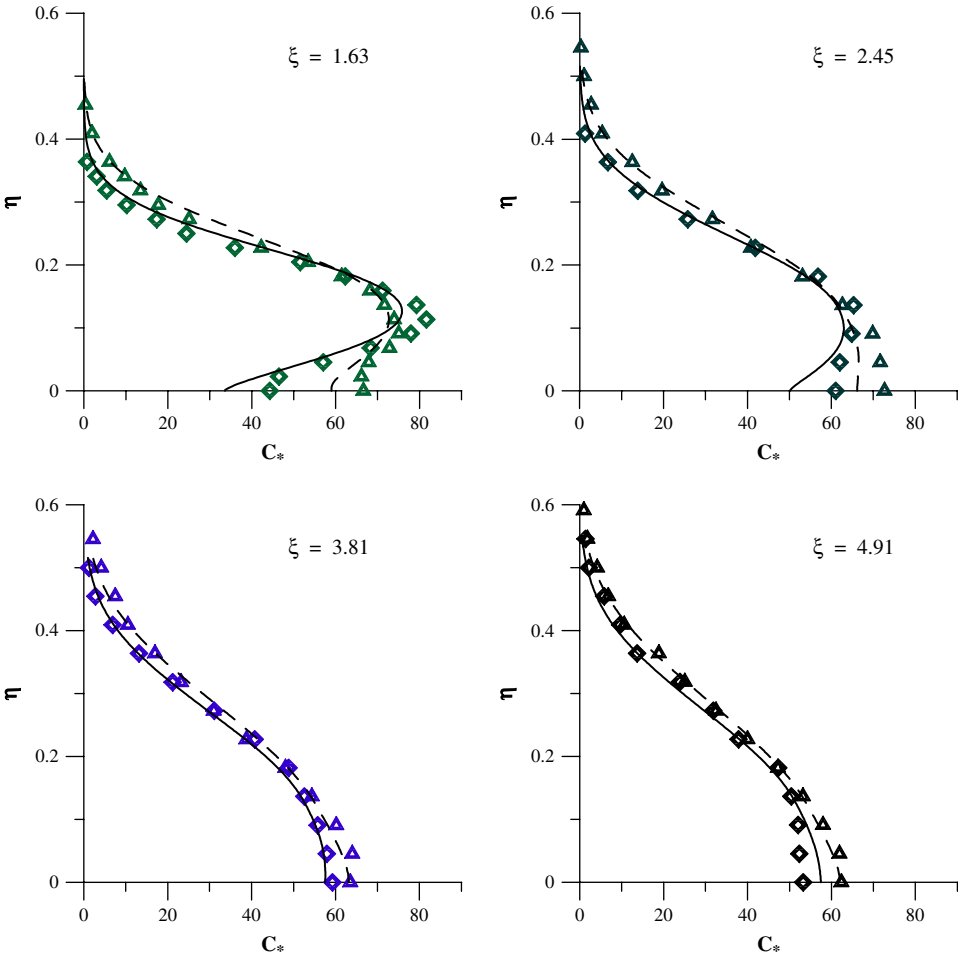

Fig. 8. Vertical profiles of concentration. Configurations 1a and 1b; source position $z_s = 2H$. Same symbols as Fig. 7.

the plume centreline, upwards and downwards, also explains why the peak concentration decreases with increasing roughness. The results from the numerical simulations agree reasonably well with the data, for both Configuration 1a and 1b. The increase in surface roughness is included in the numerical model through the form of the imposed velocity profile – which is that measured upstream of the source – and the measured value of the friction velocity, which is used to scale the diffusion coefficient. The numerical profiles show that the concentration varies very rapidly close to the top of the obstacles, and it might seem that the computed profiles do not satisfy the imposed bottom boundary condition $(\partial\overline{c}/\partial\eta = 0)$; an enlargement of this part of the profile, however, confirms that the boundary condition is indeed satisfied.

The vertical profile for Configuration 1 and a source height $z_s = 3H$ are shown in Fig. 8. Because the source is further from the top of the obstacles, the pollutant has only just been mixed down to the canopy top at $\xi = 1.63$ and the plume is almost symmetrical about the centreline. As for the source height $z_s = 2H$, the additional small scale roughness increases diffusion both close to the top of the obstacles and at the upper edge of the plume; as the plume moves downstream the effects of the small scale roughness becomes more pronounced – the concentrations at the obstacle height for Configuration 1b are much higher than those for Configuration 1a, and the 'well-mixed' region close to the top of the obstacles extends further. Despite the increases in concentration close to the top of the obstacles the peak concentration is higher for Configuration 1b than it is for Configuration 1a; at first sight this might seem paradoxical, since the total mass flux must be conserved, and it might be thought that, therefore, the peak concentration should decrease to compensate for the higher concentrations close to the tops of obstacles. In fact, the increased roughness reduces velocities in the lower part of the boundary layer, and in order to conserve the mass flux, the concentrations in this region have to increase to compensate for the decrease in velocity. The numerical solutions agree reasonably well with the data for the concentrations above the centreline, but the agreement is less satisfactory close to the top of the obstacles; for Configuration 1a the numerical simulation over-estimates the near-ground concentrations slightly, whereas for Configuration 1b it under estimates them.

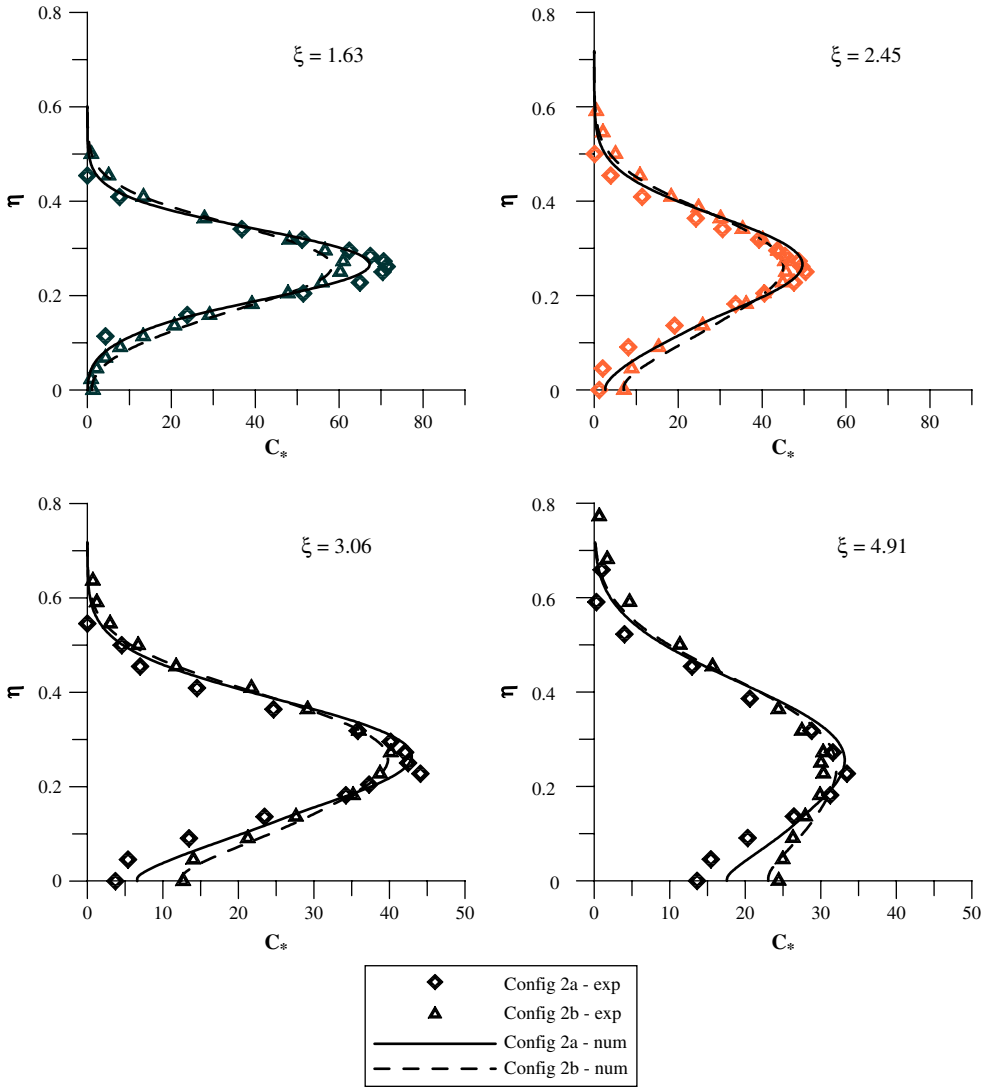

Fig. 9. Vertical profiles of concentration. Configurations 2a and 2b; source position $z_s = 3H$.

The vertical profiles of concentration for Configuration 2 ($H/W = 1/2$) are shown in Fig. 9 (for a source height $z_s = 2H$) and Fig. 10 (for $z_s = 3H$). The profiles are similar to those for Configuration 1 ($H/W = 1$), which can be explained principally by the fact that the flow regime (skimming flow) is the same for both configurations. However there are also some important differences. Close to the source the concentrations at the tops of the obstacles for Configuration 2 are significantly lower than those for Configuration 1, although the profiles have been measured at the same distance downstream of the source ($\xi = 1.36$). Much further downstream the concentration profiles are identical, so the long time diffusion for the two configurations is the same, and does not depend on the small-scale roughness. The two configurations differ in the width of the cavities between the obstacles – the cavities in Configuration 2 are half the width of the cavities in Configuration 1. The mixing close to the top of the obstacles will depend principally on the turbulence generated in the mixing layer at the top of each cavity. And since the characteristic size of the eddies in a mixing layer increases with distance from the origin, the turbulent intensity at the cavity top will increase with the width of the cavity. So the mixing at the obstacles height in Configuration 2 is less than in Configuration 1 for two reasons: firstly, the cavities are shorter in Configuration 2 and secondly, for the same distance downstream from the source, more of the lower boundary is occupied by the tops of obstacles than in Configuration 1. Further downstream the plume diffusion is dominated by the large-scale structures in the boundary layer, which are not influenced by the detailed structure of the boundary, so the concentration profiles become similar, and independent of the small scale roughness.

The concentration profiles for the wake-interference regime (Figs. 11 and 12) show that the small-scale roughness has negligible influence on the concentrations. The profiles obtained by solving the advection–diffusion equation with a two-layer diffusivity (K_{IR}) underestimate the

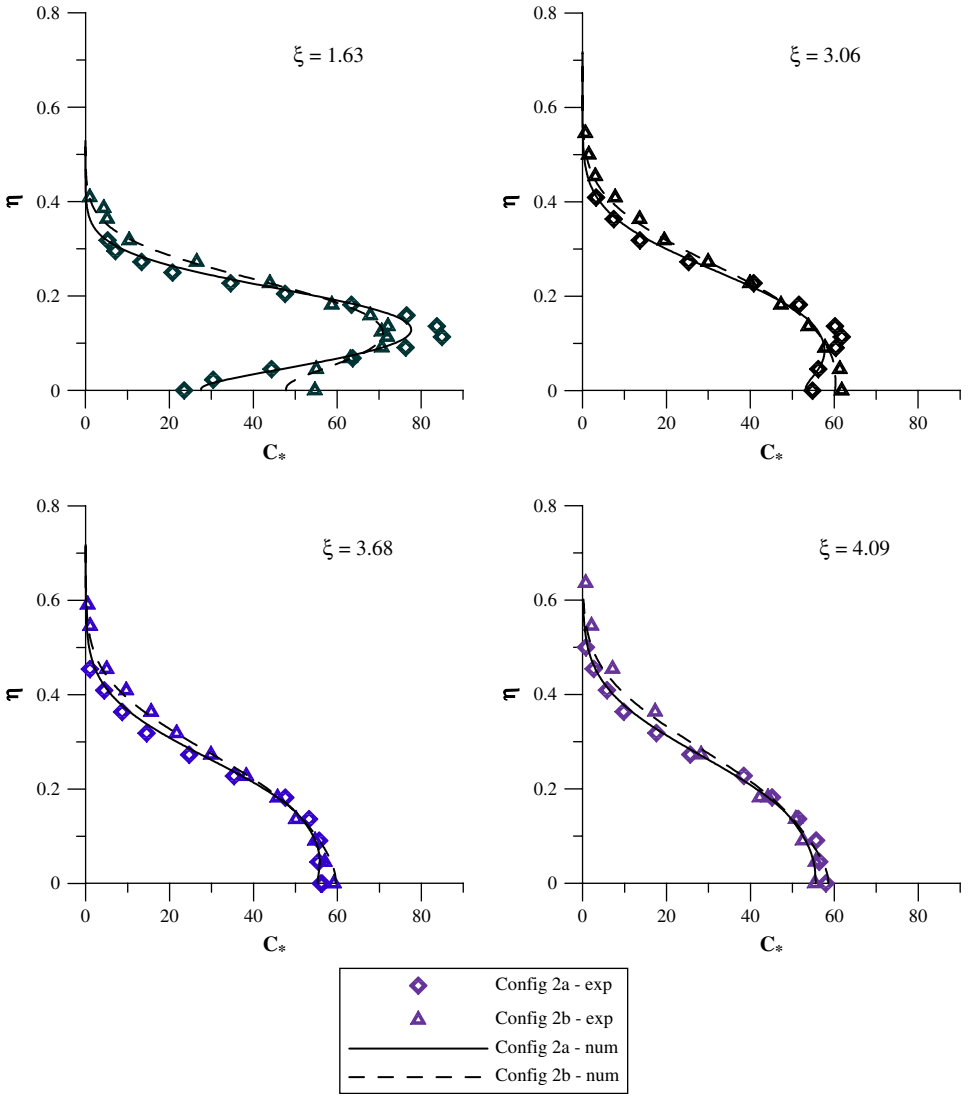

Fig. 10. Vertical profiles of concentration. Configurations 2a and 2b; source position $z_s = 2H$.

concentrations close to the top of the obstacles, except for the two profiles further downstream ($\xi = 4.09$ and $\xi = 4.91$) for a source height of $2H$, for which the numerical model over-estimates the concentrations. The RSL is much thicker in this configuration and its influence on the dispersion must be taken into account. Other studies have already shown that the momentum diffusivity in the RSL is greater than that given by a simple linear increase in diffusivity with distance from the boundary, as in the inertial layer, and this has been attributed to the presence of large scale structures (Raupach et al., 1980; Bandyopadhyay and Watson, 1988). In our experiments this additional diffusivity must come from the large-scale roughness elements rather than the small scale roughness, since the concentrations do not change with small scale roughness. The structures that are primarily responsible for this will be those formed in the wakes of the large obstacles. To include these effects we assume that the diffusivity in the RSL is constant with height, and uniform in the horizontal plane, so that it represents a form of spatially averaged (Raupach and Shaw, 1982) diffusion coefficient for the RSL. We assume that the diffusion coefficient for the RSL scales on the height of the obstacles and the friction velocity, so that K^+ takes the form (Fig. 13):

$$0 < \eta < \eta_1 \quad K^+ = \kappa \frac{H}{\delta - H} \frac{u_*}{U_\infty} \tag{8}$$

$$\eta_1 < \eta < \eta_2 \quad K^+(\eta) = \kappa \frac{u_*}{U_\infty} \eta \tag{9}$$

$$\eta_2 < \eta < 1 \quad K^+ = \alpha \frac{u_*}{U_\infty} \tag{10}$$

The use of a constant diffusivity for the roughness sub-layer is probably a simplification – this corresponds to a constant

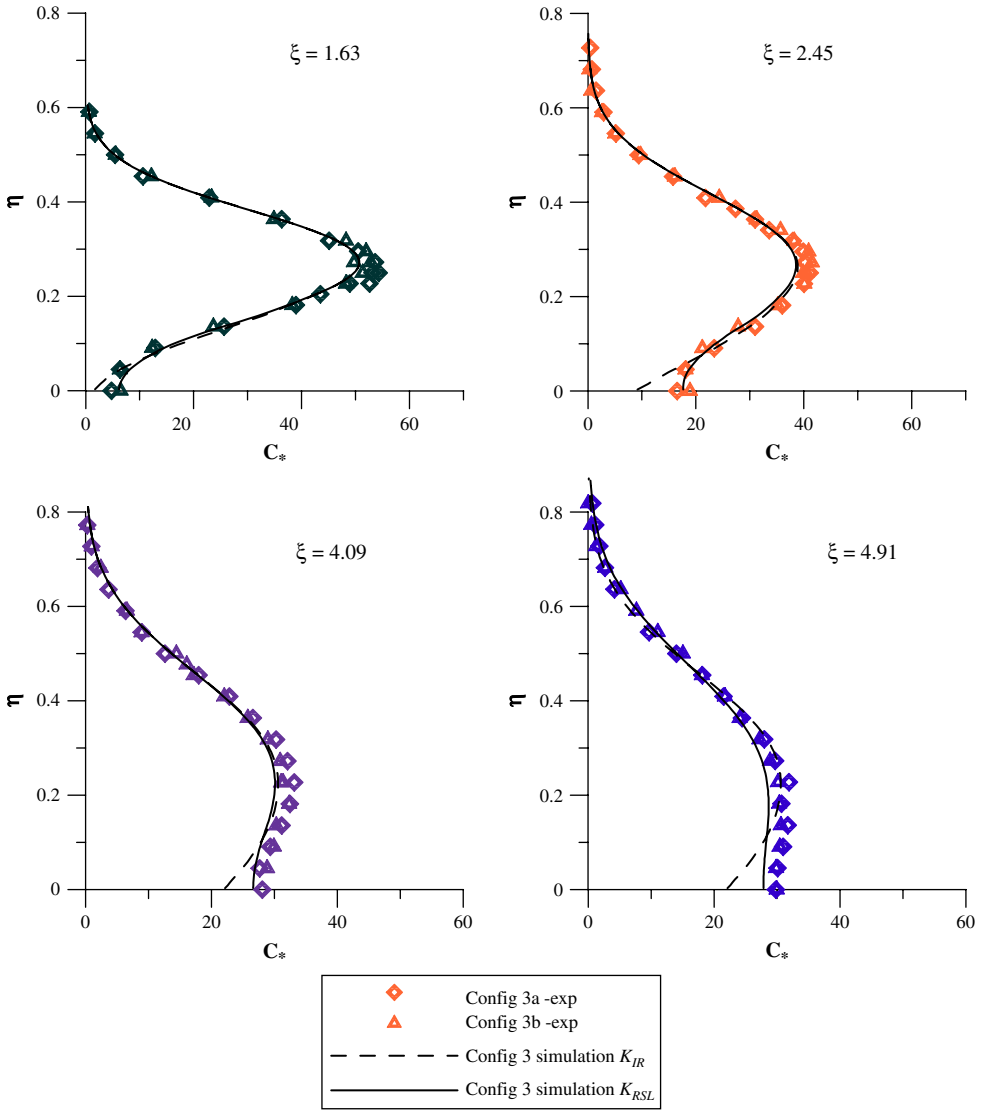

Fig. 11. Vertical profiles of concentration. Configurations 3a and 3b; source position $z_s = 3H$. K_{IR}: simulations without the RSL; K_{RSL}: simulations with the RSL.

length scale for the turbulence in the RSL, independent of distance from the tops of obstacles, whereas wind tunnel (Salizzoni, 2006) and open field (Christen et al., 2007) measurements show that the integral length scale increases linearly with distance from the tops of obstacles. But the diffusivity will not go to zero at the tops of the obstacles, because of the influence of the turbulence generated in the mixing layers over the cavities, and it is possible that the increase in length scales over the depth of the RSL is small enough for the diffusivity to be modelled satisfactorily by a constant value.

In the outer region $\alpha = 0.07$; this was obtained using a similar approach to that adopted for the two-layer model. We have assumed that the appropriate length scale for the diffusivity in the RSL is the obstacle height H, and that the length scale in the region between the RSL and the outer region varies linearly with distance from the canopy top. Then continuity of the diffusion coefficient implies that $\eta_1 = H/(\delta - H) = 0.137$. As before, continuity of the diffusion coefficient at the interface between the outer region and the IR requires $\eta_2 = \alpha/\kappa$; simulations were carried out with different values of α (and hence η_2) to choose the value that gave the best agreement with the data. On this basis we obtained $\alpha = 0.07 \pm 0.005$, from which $\eta_2 = 0.175$ which is a bit less than the value obtained for the outer limit of the inertial layer from Reynolds stress measurements $\eta_r = 0.22$ (Table 1). For all three configurations, the outer limit of the variable diffusion coefficient is slightly less than the corresponding value for the boundary of the IR. The value of $\alpha = 0.07$ is slightly higher than the corresponding value for Configurations 1 and 2 (where $\alpha = 0.05$) and indicates that in this regime (wake-interference) the diffusion in the outer region is enhanced by the large scale roughness. This also shows that the value of δ/h_s is not large enough to ensure that wall similarity applies.

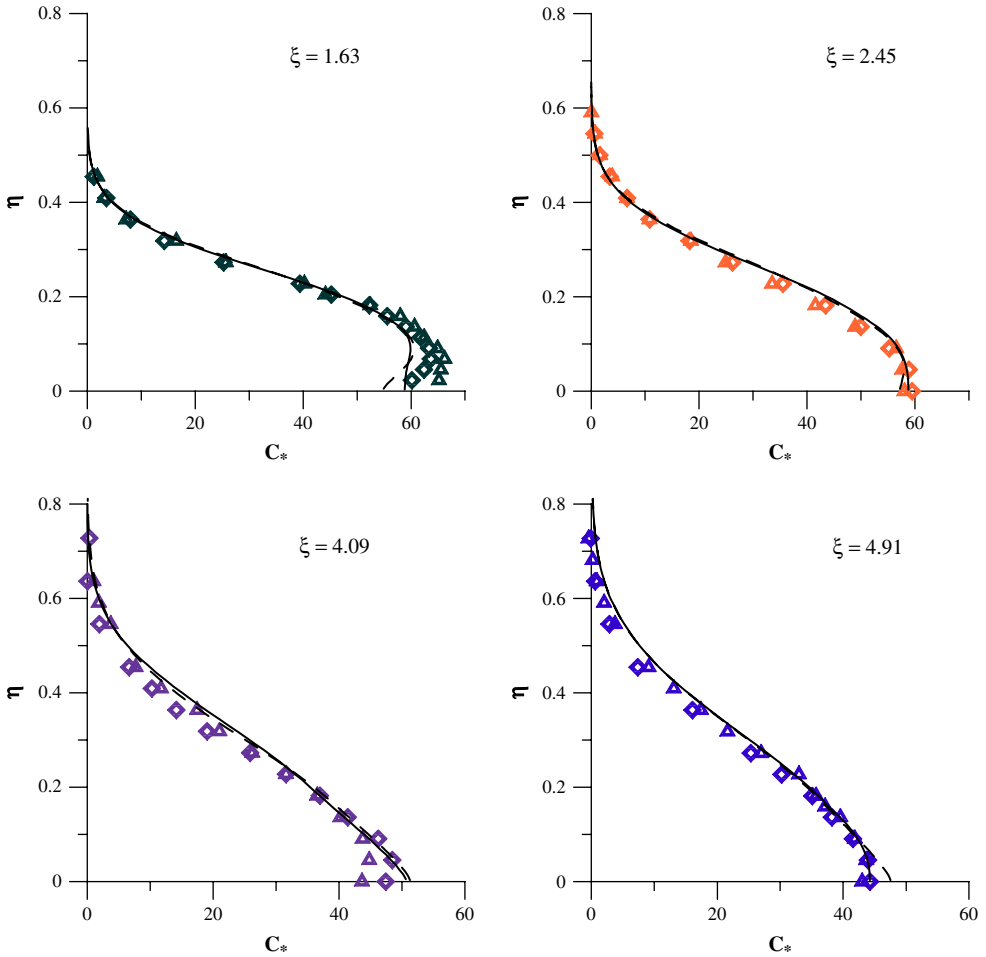

Fig. 12. Vertical profiles of concentration. Configurations 3a and 3b; source position $z_s = 2H$. K_{IR}: simulations without the RSL; K_{RSL}: simulations with the RSL. Same symbols as Fig. 11.

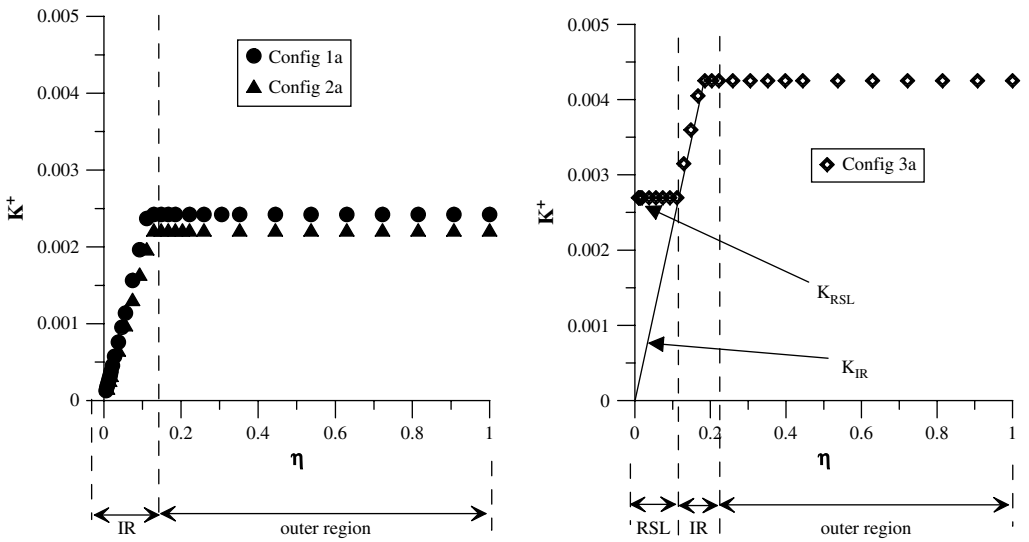

Fig. 13. Vertical profiles of the modelled normalised dispersion coefficient K^+.

The concentration profiles plotted in Figs. 11 and 12 show that the three-layer model for the diffusivity gives a much better prediction of the measured concentrations, particularly close to the tops of the obstacles. In general the three-layer diffusivity (K_{RSL}) reproduces the concentrations at the tops of the obstacles rather well, and much better than the two-layer model K_{IR}, for both source heights and all positions downstream of the source. The only noticeable difference between the data and the simulations occurs for a source height $z_s = 2H$ at a distance downstream $\xi = 4.09$, for which both models (K_{RSL} and K_{IR}) overestimate the concentration at the obstacle top.

The three-layer model also provides reasonable predictions of the concentrations throughout the RSL; the only exception to this occurs close to the source, for a source height $z_s = 2H$ (Fig. 12), where the concentrations are underpredicted. This is probably due to the use of a constant diffusivity in the RSL; the source is located at the top of the RSL ($\eta_s = z_s/(\delta - H) \sim 0.137$) and the near-field diffusion will be very sensitive to the form of the diffusivity profile. The simulation with the two-layer diffusivity profile (K_{IR}), for which the diffusivity varies linearly with distance from the obstacle tops, reproduces the form of the concentration profile correctly, but the concentrations are too low. So a linear profile of diffusivity, with a non-zero value at the obstacle height, would probably improve the near-field concentration profile for the lower source.

6. Conclusions

The influence of roughness on the dispersion above a series of cavities has been studied using wind tunnel experiments and numerical simulations. Different wall roughnesses were obtained by varying the cavity aspect ratios H/W and by adding smaller scale roughness at the top of the bars. As expected, decreasing the cavity aspect ratio induces higher turbulent mass fluxes. The addition of small roughnesses enhances the turbulent fluxes, but only in the skimming flow regime, where the large-scale obstacles are packed sufficiently closely together. This is similar to what has been observed in velocity measurements (Salizzoni et al., 2008).

Numerical simulations have been performed, assuming a turbulent diffusivity $K(z) = \ell(z)v(z)$. Based on similarity theory, the domain was decomposed into three regions (outer layer, inertial layer and roughness sub-layer) and appropriate scalings for $v(z)$ and $\ell(z)$ were defined for each layer. Comparisons with data show that a first order model for the dispersion coefficient can provide reasonable estimates for dispersion.

In the numerical simulations, the role of the wall roughness was taken into account only by varying the friction velocity. This suggests that the dispersion process within the boundary layer flow is not directly related to the spatial scale imposed at the wall but mainly to the characteristic scaling of the boundary layer flow. The results show that outside the RSL the dispersion coefficient only scales on δ, z and u_*, as predicted by similarity theory. This conclusion is valid for sufficiently deep plumes, whose extent exceeds the typical roughness length scale. This does not hold in the RSL, where the inhomogeneities in the flow become important. In the wake-interference regime the obstacles have much more influence on the flow – the thickness of the RSL increases by a factor of 6, and the height of the upper limit of the inertial layer by a factor 1.5. The influence of the obstacles extends further up into the flow, and this is reflected in an increased value of the integral length scale used to estimate the diffusivity in the outer region – α increases from 0.05 for skimming flow to 0.07 for the wake-interference regime. A simple model for a spatially averaged dispersion coefficient in the RSL has been proposed, which provides a good prediction of concentrations at the top of the modelled urban canopy. The results from simulations of scalar dispersion suggest that the enhanced diffusivity within the RSL is due to an increase in the integral length scale. In the wake-interference regime, this seems to scale with the obstacle height, H, but the near-field measurements for a source close to the ground suggest that a linear profile with a non-zero value at the obstacle tops might be an even better model.

The proposed model for dispersion in the RSL has only been tested for a few very simple geometries, and it needs to be tested for more complex configurations.

Appendix. Supplementary data

Supplementary data associated with this article can be found in the online version at doi:10.1016/j.atmosenv.2008.07.057.

References

Bandyopadhyay, P.R., Watson, R.D., 1988. Structure of rough-wall turbulent boundary layers. Physics Fluids 31 (7), 1877–1883.

Belcher, S.E., Jerram, N., Hunt, J.C.R., 2003. Adjustment of a turbulent boundary layer to a canopy of roughness elements. Journal of Fluid Mechanics 488, 369–398.

Bott, A., 1989a. A positive definite advection scheme obtained by nonlinear renormalization of the advective fluxes. Monthly Weather Review 117, 1006–1015.

Bott, A., 1989b. Reply. Monthly Weather Review 117, 2633–2636.

Britter, R., Hanna, S., 2003. Flow and dispersion in urban areas. Annual Review of Fluid Mechanics 35, 469–496.

Builtjes, P., 1984. Determination of the flow and concentration field in a street canyon by means of wind tunnel experiments. Tech. Rep. 84–02616, TNO – Netherlands.

Clarke, R.H., 1970. Observational studies in the atmospheric boundary layer. Quarterly Journal of the Royal Meteorological Society 96, 91–114.

Christen, A., van Gorsel, E., Vogt, R., 2007. Coherent structures in urban roughness sub layer turbulence. International Journal of Climatology 27, 1955–1968.

Coppin, P., Raupach, M., Legg, B., 1986. Experiments on scalar dispersion within a model plant canopy part II: an elevated plane source. Boundary-Layer Meteorology 35, 167–191.

Davidson, M.J., Mylne, K.R., Jones, C.D., Phillips, J.C., Perkins, R., 1995. Plume dispersion through large groups of obstacles – a field investigation. Atmospheric Environment 29 (22), 3245–3256.

Fackrell, J.E., 1980. A flame ionisation detector for measuring fluctuating concentration. Journal of Physics E Scientific Instruments 13, 888–893.

Fackrell, J.E., Robins, A.G., 1982. Concentration fluctuations and fluxes in plumes from point sources in a turbulent boundary layer. Journal of Fluid Mechanics 117, 1–26.

Garratt, J.R., 1978. Flux profile relations above tall vegetation. Quarterly Journal of the Royal Meteorological Society 104, 199–211.

Irwin, H.P.A.H., 1981. The design of spires for wind simulation. Journal of Wind Engineering and Industrial Aerodynamics 7, 361–366.

Jiménez, J., 2004. Turbulent flows over rough wall. Annual Review of Fluid Mechanics 36, 173–196.

Kastner-Klein, P., Fedorovich, E., Rotach, M., 2004. Mean flow and turbulence characteristics in an urban roughness sub layer. Boundary-Layer Meteorology 111, 55–84.

Kitabayashi, K., Sugawara, K., Isomura, S., 1976. A wind tunnel study of automobile exhaust gas diffusion in an urban district. In: Fourth Int. Clean Air Congr, vol. II–15, 192–195.

Nikuradse, J., 1933. Strömungsgesetze in rauhen rohren. Forschg. Arb. Ing.-Wes 361.

Oke, T.R., 1988. Boundary layer climates. The Meteorological Magazine 117 (1394).

Raupach, M., Coppin, P., 1983. Turbulent dispersion from an elevated line source: measurements of wind concentration moments and budgets. Journal of Fluid Mechanics 136, 111–137.

Raupach, M.R., Coppin, P.A., Legg, B.J., 1986. Experiments on scalar dispersion within a model plant canopy. Part I: the turbulence structure. Boundary-Layer Meteorology 35, 21–52.

Raupach, M.R., Shaw, R.H., 1982. Averaging procedures for flow within vegetation canopies. Boundary-Layer Meteorology 22, 79–90.

Raupach, M.R., Thom, A.S., Edwards, I., 1980. A wind-tunnel study of turbulent flow close to regularly arrayed rough surfaces. Boundary-Layer Meteorology 18, 373–397.

Rotach, M.W., 1995. Profiles of turbulence statistics in and above an urban street canyon. Atmospheric Environment 29 (13), 1473–1486.

Salizzoni, P., 2006. Mass and momentum transfer in the urban boundary layer. Ph.D. thesis, Politecnico di Torino – Ecole Centrale de Lyon, 186 p.

Salizzoni, P., Soulhac, L., Mejean, P., Perkins, R., 2008. Influence of a two scale surface roughness on a turbulent boundary layer. Boundary-Layer Meteorology 127, 97–110.

Taylor, G., 1954. The dispersion of matter in turbulent flow through a pipe. Proceedings of the Royal Society A 223, 446–468.

Thom, A.S., 1971. Momentum absorption by vegetation. Quarterly Journal of the Royal Meteorological Society 97, 414–428.

Thuburn, J., 1997. TVD schemes, positive schemes, and the universal limiter. Monthly Weather Review 125, 1990–1993.